Measurement of single electron event anisotropy in Au+Au collisions at $\sqrt{s_{NN}} = 200$ GeV

S. S. Adler,[5] S. Afanasiev,[17] C. Aidala,[5] N. N. Ajitanand,[43] Y. Akiba,[20,38] J. Alexander,[43] R. Amirikas,[12] L. Aphecetche,[45] S. H. Aronson,[5] R. Averbeck,[44] T. C. Awes,[35] R. Azmoun,[44] V. Babintsev,[15] A. Baldisseri,[10] K. N. Barish,[6] P. D. Barnes,[27] B. Bassalleck,[33] S. Bathe,[30] S. Batsouli,[9] V. Baublis,[37] A. Bazilevsky,[39,15] S. Belikov,[16,15] Y. Berdnikov,[40] S. Bhagavatula,[16] J. G. Boissevain,[27] H. Borel,[10] S. Borenstein,[25] M. L. Brooks,[27] D. S. Brown,[34] N. Bruner,[33] D. Bucher,[30] H. Buesching,[30] V. Bumazhnov,[15] G. Bunce,[5,39] J. M. Burward-Hoy,[26,44] S. Butsyk,[44] X. Camard,[45] J.-S. Chai,[18] P. Chand,[4] W. C. Chang,[2] S. Chernichenko,[15] C. Y. Chi,[9] J. Chiba,[20] M. Chiu,[9] I. J. Choi,[52] J. Choi,[19] R. K. Choudhury,[4] T. Chujo,[5] V. Cianciolo,[35] Y. Cobigo,[10] B. A. Cole,[9] P. Constantin,[16] D. d'Enterria,[45] G. David,[5] H. Delagrange,[45] A. Denisov,[15] A. Deshpande,[39] E. J. Desmond,[5] A. Devismes,[44] O. Dietzsch,[41] O. Drapier,[25] A. Drees,[44] K. A. Drees,[5] R. du Rietz,[29] A. Durum,[15] D. Dutta,[4] Y. V. Efremenko,[35] K. El Chenawi,[49] A. Enokizono,[14] H. En'yo,[38,39] S. Esumi,[48] L. Ewell,[5] D. E. Fields,[33,39] F. Fleuret,[25] S. L. Fokin,[23] B. D. Fox,[39] Z. Fraenkel,[51] J. E. Frantz,[9] A. Franz,[5] A. D. Frawley,[12] S.-Y. Fung,[6] S. Garpman,[29,*] T. K. Ghosh,[49] A. Glenn,[46] G. Gogiberidze,[46] M. Gonin,[25] J. Gosset,[10] Y. Goto,[39] R. Granier de Cassagnac,[25] N. Grau,[16] S. V. Greene,[49] M. Grosse Perdekamp,[39] W. Guryn,[5] H.-Å. Gustafsson,[29] T. Hachiya,[14] J. S. Haggerty,[5] H. Hamagaki,[8] A. G. Hansen,[27] E. P. Hartouni,[26] M. Harvey,[5] R. Hayano,[8] N. Hayashi,[38] X. He,[13] M. Heffner,[26] T. K. Hemmick,[44] J. M. Heuser,[44] M. Hibino,[50] J. C. Hill,[16] W. Holzmann,[43] K. Homma,[14] B. Hong,[22] A. Hoover,[34] T. Ichihara,[38,39] V. V. Ikonnikov,[23] K. Imai,[24,38] D. Isenhower,[1] M. Ishihara,[38] M. Issah,[43] A. Isupov,[17] B. V. Jacak,[44] W. Y. Jang,[22] Y. Jeong,[19] J. Jia,[44] O. Jinnouchi,[38] B. M. Johnson,[5] S. C. Johnson,[26] K. S. Joo,[31] D. Jouan,[36] S. Kametani,[8,50] N. Kamihara,[47,38] J. H. Kang,[52] S. S. Kapoor,[4] K. Katou,[50] S. Kelly,[9] B. Khachaturov,[51] A. Khanzadeev,[37] J. Kikuchi,[50] D. H. Kim,[31] D. J. Kim,[52] D. W. Kim,[19] E. Kim,[42] G.-B. Kim,[25] H. J. Kim,[52] E. Kistenev,[5] A. Kiyomichi,[48] K. Kiyoyama,[32] C. Klein-Boesing,[30] H. Kobayashi,[38,39] L. Kochenda,[37] V. Kochetkov,[15] D. Koehler,[33] T. Kohama,[14] M. Kopytine,[44] D. Kotchetkov,[6] A. Kozlov,[51] P. J. Kroon,[5] C. H. Kuberg,[1,27] K. Kurita,[39] Y. Kuroki,[48] M. J. Kweon,[22] Y. Kwon,[52] G. S. Kyle,[34] R. Lacey,[43] V. Ladygin,[17] J. G. Lajoie,[16] A. Lebedev,[16,23] S. Leckey,[44] D. M. Lee,[27] S. Lee,[19] M. J. Leitch,[27] X. H. Li,[6] H. Lim,[42] A. Litvinenko,[17] M. X. Liu,[27] Y. Liu,[36] C. F. Maguire,[49] Y. I. Makdisi,[5] A. Malakhov,[17] V. I. Manko,[23] Y. Mao,[7,38] G. Martinez,[45] M. D. Marx,[44] H. Masui,[48] F. Matathias,[44] T. Matsumoto,[8,50] P. L. McGaughey,[27] E. Melnikov,[15] F. Messer,[44] Y. Miake,[48] J. Milan,[43] T. E. Miller,[49] A. Milov,[44,51] S. Mioduszewski,[5] R. E. Mischke,[27] G. C. Mishra,[13] J. T. Mitchell,[5] A. K. Mohanty,[4] D. P. Morrison,[5] J. M. Moss,[27] F. Mühlbacher,[44] D. Mukhopadhyay,[51] M. Muniruzzaman,[6] J. Murata,[38,39] S. Nagamiya,[20] J. L. Nagle,[9] T. Nakamura,[14] B. K. Nandi,[6] M. Nara,[48] J. Newby,[46] P. Nilsson,[29] A. S. Nyanin,[23] J. Nystrand,[29] E. O'Brien,[5] C. A. Ogilvie,[16] H. Ohnishi,[5,38] I. D. Ojha,[49,3] K. Okada,[38] M. Ono,[48] V. Onuchin,[15] A. Oskarsson,[29] I. Otterlund,[29] K. Oyama,[8] K. Ozawa,[8] D. Pal,[51] A. P. T. Palounek,[27] V. Pantuev,[44] V. Papavassiliou,[34] J. Park,[42] A. Parmar,[33] S. F. Pate,[34] T. Peitzmann,[30] J.-C. Peng,[27] V. Peresedov,[17] C. Pinkenburg,[5] R. P. Pisani,[5] F. Plasil,[35] M. L. Purschke,[5] A. K. Purwar,[44] J. Rak,[16] I. Ravinovich,[51] K. F. Read,[35,46] M. Reuter,[44] K. Reygers,[30] V. Riabov,[37,40] Y. Riabov,[37] G. Roche,[28] A. Romana,[25] M. Rosati,[16] P. Rosnet,[28] S. S. Ryu,[52] M. E. Sadler,[1] N. Saito,[38,39] T. Sakaguchi,[8,50] M. Sakai,[32] S. Sakai,[48] V. Samsonov,[37] L. Sanfratello,[33] R. Santo,[30] H. D. Sato,[24,38] S. Sato,[5,48] S. Sawada,[20] Y. Schutz,[45] V. Semenov,[15] R. Seto,[6] M. R. Shaw,[1,27] T. K. Shea,[5] T.-A. Shibata,[47,38] K. Shigaki,[14,20] T. Shiina,[27] C. L. Silva,[41] D. Silvermyr,[27,29] K. S. Sim,[22] C. P. Singh,[3] V. Singh,[3] M. Sivertz,[5] A. Soldatov,[15] R. A. Soltz,[26] W. E. Sondheim,[27] S. P. Sorensen,[46] I. V. Sourikova,[5] F. Staley,[10] P. W. Stankus,[35] E. Stenlund,[29] M. Stepanov,[34] A. Ster,[21] S. P. Stoll,[5] T. Sugitate,[14] J. P. Sullivan,[27] E. M. Takagui,[41] A. Taketani,[38,39] M. Tamai,[50] K. H. Tanaka,[20] Y. Tanaka,[32] K. Tanida,[38] M. J. Tannenbaum,[5] P. Tarján,[11] J. D. Tepe,[1,27] T. L. Thomas,[33] J. Tojo,[24,38] H. Torii,[24,38] R. S. Towell,[1] I. Tserruya,[51] H. Tsuruoka,[48] S. K. Tuli,[3] H. Tydesjö,[29] N. Tyurin,[15] H. W. van Hecke,[27] J. Velkovska,[5,44] M. Velkovsky,[44] V. Veszprémi,[11] L. Villatte,[46] A. A. Vinogradov,[23] M. A. Volkov,[23] E. Vznuzdaev,[37] X. R. Wang,[13] Y. Watanabe,[38,39] S. N. White,[5] F. K. Wohn,[16] C. L. Woody,[5] W. Xie,[6] Y. Yang,[7] A. Yanovich,[15] S. Yokkaichi,[38,39] G. R. Young,[35] I. E. Yushmanov,[23] W. A. Zajc,[9,†] C. Zhang,[9] S. Zhou,[7] S. J. Zhou,[51] and L. Zolin[17]

(PHENIX Collaboration)

[1]*Abilene Christian University, Abilene, Texas 79699, USA*

[2]*Institute of Physics, Academia Sinica, Taipei 11529, Taiwan*

[3]*Department of Physics, Banaras Hindu University, Varanasi 221005, India*

[4]*Bhabha Atomic Research Centre, Bombay 400 085, India*

[5]*Brookhaven National Laboratory, Upton, New York 11973-5000, USA*

[6]*University of California, Riverside, California 92521, USA*

[7]*China Institute of Atomic Energy (CIAE), Beijing, People's Republic of China*

[8]*Center for Nuclear Study, Graduate School of Science, University of Tokyo, 7-3-1 Hongo, Bunkyo, Tokyo 113-0033, Japan*

[9]*Columbia University, New York, New York 10027 and Nevis Laboratories, Irvington, New York 10533, USA*

[10]*Dapnia, CEA Saclay, F-91191, Gif-sur-Yvette, France*

[11]*Debrecen University, Egyetem tér 1, H-4010 Debrecen, Hungary*

[12]*Florida State University, Tallahassee, Florida 32306, USA*

[13]*Georgia State University, Atlanta, Georgia 30303, USA*

[14]*Hiroshima University, Kagamiyama, Higashi-Hiroshima 739-8526, Japan*

[15]*Institute for High Energy Physics (IHEP), Protvino, Russia*

[16]*Iowa State University, Ames, Iowa 50011, USA*
[17]*Joint Institute for Nuclear Research, 141980 Dubna, Moscow Region, Russia*
[18]*KAERI, Cyclotron Application Laboratory, Seoul, South Korea*
[19]*Kangnung National University, Kangnung 210-702, South Korea*
[20]*KEK, High Energy Accelerator Research Organization, Tsukuba-shi, Ibaraki-ken 305-0801, Japan*
[21]*KFKI Research Institute for Particle and Nuclear Physics of the Hungarian Academy of Sciences (MTA KFKI RMKI), Post Office Box 49, H-1525 Budapest 114, Hungary*
[22]*Korea University, Seoul, 136-701, Korea*
[23]*Russian Research Center "Kurchatov Institute," Moscow, Russia*
[24]*Kyoto University, Kyoto 606-8502, Japan*
[25]*Laboratoire Leprince-Ringuet, Ecole Polytechnique, CNRS-IN2P3, Route de Saclay, F-91128, Palaiseau, France*
[26]*Lawrence Livermore National Laboratory, Livermore, California 94550, USA*
[27]*Los Alamos National Laboratory, Los Alamos, New Mexico 87545, USA*
[28]*LPC, Université Blaise Pascal, CNRS-IN2P3, Clermont-Fd, F-63177 Aubiere Cedex, France*
[29]*Department of Physics, Lund University, Box 118, SE-221 00 Lund, Sweden*
[30]*Institut für Kernphysik, University of Muenster, D-48149 Muenster, Germany*
[31]*Myongji University, Yongin, Kyonggido 449-728, South Korea*
[32]*Nagasaki Institute of Applied Science, Nagasaki-shi, Nagasaki 851-0193, Japan*
[33]*University of New Mexico, Albuquerque, New Mexico 87131, USA*
[34]*New Mexico State University, Las Cruces, New Mexico 88003, USA*
[35]*Oak Ridge National Laboratory, Oak Ridge, Tennessee 37831, USA*
[36]*IPN-Orsay, Universite Paris Sud, CNRS-IN2P3, BP1, F-91406, Orsay, France*
[37]*PNPI, Petersburg Nuclear Physics Institute, Gatchina, Leningrad Region, 188300, Russia*
[38]*RIKEN (The Institute of Physical and Chemical Research), Wako, Saitama 351-0198, Japan*
[39]*RIKEN BNL Research Center, Brookhaven National Laboratory, Upton, New York 11973-5000, USA*
[40]*St. Petersburg State Technical University, St. Petersburg, Russia*
[41]*Universidade de São Paulo, Instituto de Física, Caixa Postal 66318, São Paulo CEP05315-970, Brazil*
[42]*System Electronics Laboratory, Seoul National University, Seoul, South Korea*
[43]*Chemistry Department, Stony Brook University, SUNY, Stony Brook, New York 11794-3400, USA*
[44]*Department of Physics and Astronomy, Stony Brook University, SUNY, Stony Brook, New York 11794, USA*
[45]*SUBATECH (Ecole des Mines de Nantes, CNRS-IN2P3, Université de Nantes) Bôite Postale 20722, F-44307 Nantes, France*
[46]*University of Tennessee, Knoxville, Tennessee 37996, USA*
[47]*Department of Physics, Tokyo Institute of Technology, Oh-okayama, Meguro, Tokyo 152-8551, Japan*
[48]*Institute of Physics, University of Tsukuba, Tsukuba, Ibaraki 305, Japan*
[49]*Vanderbilt University, Nashville, Tennessee 37235, USA*
[50]*Waseda University, Advanced Research Institute for Science and Engineering, 17 Kikui-cho, Shinjuku-ku, Tokyo 162-0044, Japan*
[51]*Weizmann Institute, Rehovot 76100, Israel*
[52]*Yonsei University, IPAP, Seoul 120-749, Korea*
(Received 4 February 2005; published 10 August 2005)

The transverse momentum dependence of the azimuthal anisotropy parameter v_2, the second harmonic of the azimuthal distribution, for electrons at midrapidity ($|\eta| < 0.35$) has been measured with the PHENIX detector in Au+Au collisions at $\sqrt{s_{NN}} = 200$ GeV. The measurement was made with respect to the reaction plane defined at high rapidities ($|\eta| = 3.1$–3.9). From the result we have measured the v_2 of electrons from heavy flavor decay after subtraction of the v_2 of electrons from other sources such as photon conversions and Dalitz decay from light neutral mesons. We observe a nonzero single electron v_2 with a 90% confidence level in the intermediate-p_T region. The precision of the present data set does not permit us to conclude definitively that heavy quarks exhibit thermalization with the transverse flow of the bulk matter.

DOI: 10.1103/PhysRevC.72.024901 PACS number(s): 25.75.Dw

I. INTRODUCTION

The azimuthal anisotropy of particle emission is a powerful tool to study the early stage of ultrarelativistic nuclear collisions. The spatial anisotropy in the initial stage of noncentral nucleus-nucleus collisions is transferred into momentum anisotropy in the final state. The azimuthal anisotropy is defined by

$$\frac{dN}{d\phi} = N_0 \left\{ 1 + \sum_n 2v_n \cos[n(\phi - \Psi_{\mathrm{R.P.}})] \right\}, \qquad (1)$$

*Deceased.
†PHENIX spokesperson: zajc@nevis.columbia.edu

where N_0 is a normalization constant, ϕ is the azimuthal angle of particles, and $\Psi_{\mathrm{R.P.}}$ is the direction of the nuclear impact parameter ("reaction plane") in a given collision. The harmonic coefficients, v_n, indicate the strength of the nth anisotropy. The azimuthal anisotropy parameter v_2 (the second harmonic coefficient of the Fourier expansion of the azimuthal distribution) may be especially sensitive to the early pressure [1]. The transverse momentum (p_T) dependence of v_2 has been measured for identified particles at Brookhaven National Laboratory's Relativistic Heavy Ion Collider (RHIC) [2–5]. Previous measurements are limited to hadrons made of light quarks. These results show a clear mass dependence of v_2, which is well reproduced by a hydrodynamical calculation [6] in the low-p_T region ($p_T < 2$ GeV/c). The agreement is considered as evidence that the collective motion develops in the very early stages of the reaction. It is also observed that v_2 as a function of p_T scales via the coalescence prescription; that is, v_2/n as a function of p_T/n is universal, where n is the number of valence quarks plus valence antiquarks. This scaling behavior is consistent with the prediction of the quark coalescence model, which assumes a finite v_2 of quarks [7]. This suggests that the v_2 already develops in the partonic phase for hadrons made of light quarks. In addition, if the v_2 of heavy quarks is nonzero, it would support partonic level thermalization and very high density at the early stage of the collisions.

Electrons are a useful tool to study the production of heavy quarks such as charm quarks. In the PHENIX experiment at RHIC, transverse momentum spectra of single electrons have been measured in Au+Au collisions at $\sqrt{s_{NN}} = 130$ GeV [8] and 200 GeV [9]. The results are consistent with that expected from semileptonic charm decays in addition to decays of light mesons and photon conversions [8]. However, electrons originating from semileptonic decays of D mesons have a significant angular deviation from the original D meson direction. The effect on v_2 has been shown in [10] and [11]. The results suggest that the effect is not significant for the decay electron v_2, and the electron v_2 reflects the v_2 of the D meson. Therefore the single-electron v_2 measurement is a useful method for studying open charm v_2 [12,13].

Currently the single-electron spectra from PHENIX are consistent with two opposing scenarios: (1) initial perturbative QCD charm production without final-state interactions and (2) complete thermal equilibrium for charmed hadrons [14]. Therefore the measurement of the azimuthal anisotropy of electrons from semileptonic charm decays could give us important new information regarding the charm dynamics in high-energy heavy-ion collisions. The measurement is also important for the quark coalescence model, because of the large difference between the charm quark and light quark masses, and for the prediction of v_2 for the J/ψ and the D meson, those contain charm quarks.

In this paper, we present the first measurement of the single-electron v_2, which is expected to reflect the heavy flavor azimuthal anisotropy, below 4 GeV/c with respect to the reaction plane in Au+Au collisions at $\sqrt{s_{NN}} = 200$ GeV. The single-electron v_2 was measured by subtracting from the inclusive electron v_2 the v_2 of electrons from other sources such as photon conversions and Dalitz decays from light neutral mesons.

II. DATA ANALYSIS

About 16 million minimum bias events in RHIC-Run2 (2001) for $\sqrt{s_{NN}} = 200$ GeV are used in this analysis after a vertex cut is applied ($|z_{\mathrm{vertex}}| < 20$ cm). In this section we present a brief overview of the PHENIX detectors [15] used in this analysis and then present details of event selection, electron identification, and reaction-plane determination.

A. Overview of PHENIX detector

PHENIX consists of four spectrometer arms (central arms and muon arms) and a set of global detectors. The central arms are located east and west of the interaction region at midrapidity. The muon arms are located to the north and south at forward rapidity. Figure 1 shows the configuration of the central arms in Run2.

The global detectors consist of the beam-beam-counters (BBCs) and the zero-degree calorimeters (ZDCs). These detectors provide the time of the Au+Au collision, the collision vertex, the event trigger, and the collision centrality. In this analysis the BBCs are also used to determine the reaction plane. The BBCs are installed on the north and south sides of the collision point along the beam axis. Each BBC is placed 144 cm from the center of the interaction region and surrounds the beam pipe. This corresponds to a pseudorapidity range from 3.1 to 3.9 over the full azimuth. Each BBC is composed of 64 elements and a single BBC element consists of a 1-in-diameter mesh dynode photomultiplier tube mounted on a 3-cm-long quartz radiator. The ZDC is a hadron calorimeter and measures the energy of spectator neutrons. The ZDCs are located 18 m downstream and upstream along the beam axis, and each ZDC covers 2 mrad of forward angular cone, corresponding to $\eta > 6.0$.

The central arms are designed to track particles emitted from collisions, identify charged particles, and reconstruct invariant masses. The central arms each cover the pseudorapidity range $|\eta| < 0.35$ and 90° in azimuthal angle. The central arms consist of several subsystems. In this analysis drift chambers (DCs), pad chambers (PCs), ring imaging Cherenkov counters (RICHs), and electromagnetic calorimeters (EMCals) are used. The DCs are located between 2.0 and 2.4 m from the beam axis on each central arm and measure charged particle trajectories in the r-ϕ plane. The central arms have three layers of PCs, which are multiwire proportional chambers. The PCs are located at 2.4 m (PC1), 4.2 m (PC2), and 5.0 m (PC3) from the beam axis. PC1 and PC3 are installed in each central arm, but PC2 is installed only in the west arm. The PC measures three-dimensional space points along the straight-line particle trajectories. A RICH, the primary detector for electron identification, is installed in each central arm. The RICH consists of a gas vessel, a thin reflector, and a photon detector consisting of an array of photomultiplier tubes (PMTs). During Run2 CO_2 was used as the Cherenkov radiator so only pions with $p > 4.7$ GeV/c emit Cherenkov light in the

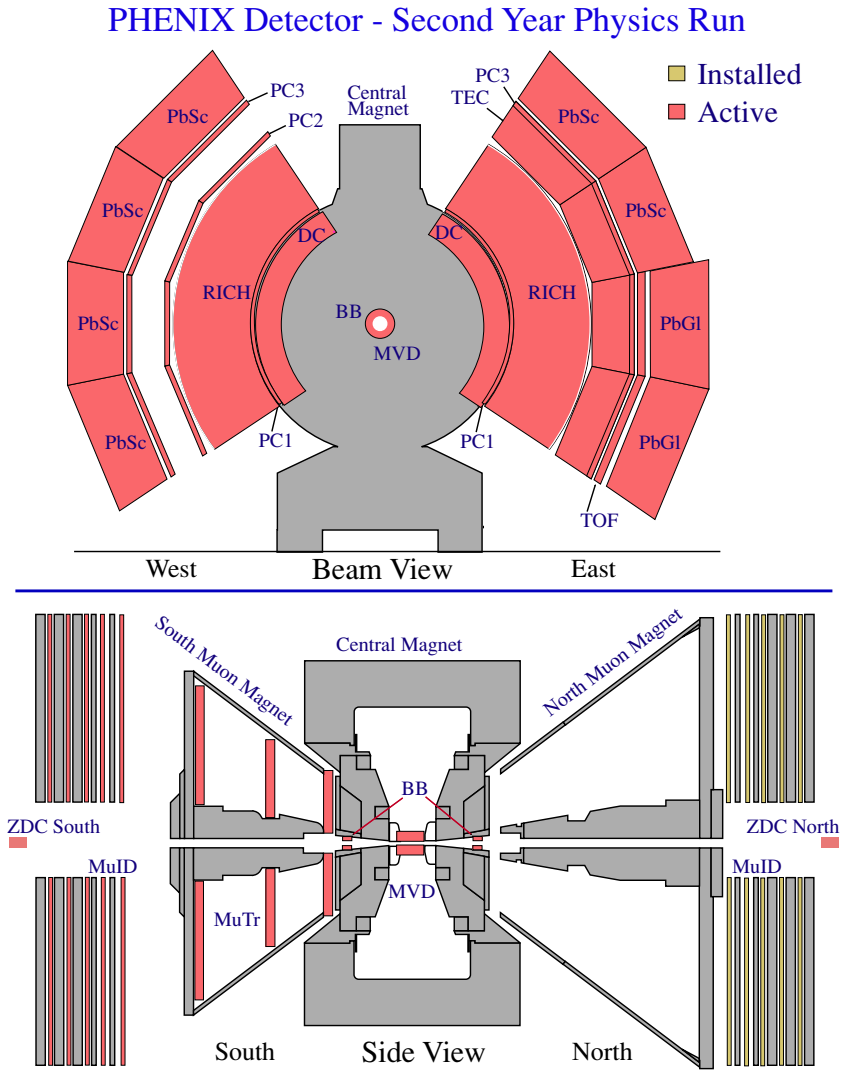

FIG. 1. (Color online) PHENIX experiment configuration in Run2. (Top) Cross section perpendicular to the beam pipe. (Bottom) East side view of the cross section along the beam pipe.

RICH. The EMCal is used to measure the spatial position and energy of electrons and photons. It covers the full central arm acceptance of $70^\circ < \theta < 110^\circ$ with each of the two walls subtending 90° in azimuth. One wall comprises four sectors of Pb-scintillator sampling calorimeter; the other has two sectors of Pb scintillator and two of Pb-glass Cherenkov calorimeter. The central magnet (CM) provides a magnetic field around the interaction vertex that is parallel to the beam. The CM allows momentum analysis of charged particles in the polar angle range $70^\circ < \theta < 110^\circ$ and provides a field integral of about 0.8 T m [16].

B. Event selection

Event selection was done with the BBC and the ZDC in this analysis. The minimum-bias trigger requires a coincidence between north and south BBC signals. The trigger included $92.2^{+2.5}_{-3.0}\%$ of the 6.9-b Au+Au inelastic cross section [17]. The event centrality is determined by combining information on spectator neutrons measured by the ZDC and the charge sum information measured by the BBC. The collision vertex point along the beam line is determined by the timing difference of the two BBCs. We required $|z_{\text{vertex}}| < 20$ cm for this analysis.

C. Charged particle selection and electron identification

Charged particle tracks are reconstructed by the DC and the first pad chamber plane (PC1) installed in each central arm together with the collision vertex determined by the BBC [18]. For a reconstructed track to be selected, the track projection to the EMCal and the position of the associated hit in the EMCal must match within two standard deviations. The electron candidates are required to have at least three associated hits in the RICH that pass a ring-shape cut and are also required to pass a timing cut. To reduce background from hadrons and photon conversions far from the vertex, energy is measured in the EMCal, and momentum matching (E/p) is required. Electrons deposit all of their energy in the EMCal; therefore the E/p is approximately 1.0. In this analysis we require $-2\sigma < (E-p)/p < 3\sigma$ to reduce background. Figure 2 shows the $(E-p)/p/\sigma$ distribution. Here the σ means a standard deviation of $(E-p)/p$. A background of less than 10% remains, caused by accidental association of

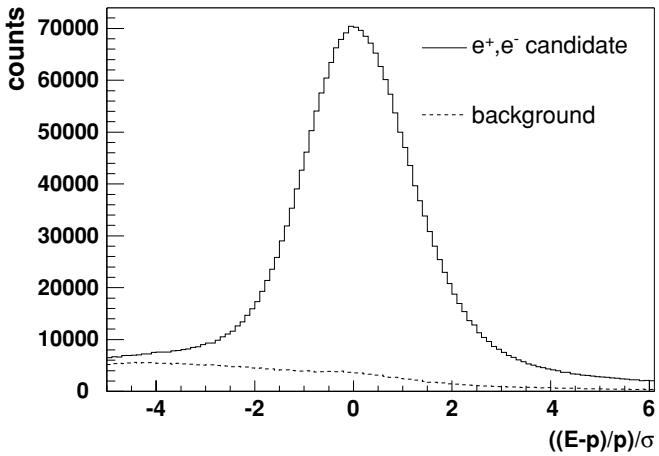

FIG. 2. $(E-p)/p/\sigma$ distribution. We require $-2\sigma < (E-p)/p < 3\sigma$ to reduce background from hadrons and photon conversions far from the vertex.

tracks with RICH hits. The background level is estimated by an event-mixing method and is subtracted when we calculate the electron v_2.

D. Reaction-plane determination

In this analysis the values of v_2 are calculated by the reaction-plane method, which measures the azimuthal angle of the particle emission with respect to the reaction plane [19]. The azimuthal angle of the reaction plane for the nth harmonic is determined by [19]

$$\psi_n^{\text{meas}} = \left[\tan^{-1}\frac{\sum_i w_i \sin(n\phi_i)}{\sum_i w_i \cos(n\phi_i)}\right] \Big/ n, \tag{2}$$

where ϕ_i is the azimuthal angle of each particle used in the reaction-plane determination and w_i is the corresponding weight. The azimuthal angle distribution of the particle emission measured with respect to the reaction plane can be written as Eq. (1). Because of finite reaction-plane resolution, coefficients in the Fourier expansion of the azimuthal distribution with respect to the "measured" reaction plane (v_n^{meas}) are smaller than coefficients measured with respect to the "real" reaction plane (v_n). The resolution correction necessary for v_n^{meas} is given by

$$v_n = v_n^{\text{meas}}/\sigma_{v_n}, \tag{3}$$

where v_n is the real coefficient and σ_{v_n} is the reaction-plane resolution for the nth harmonic. The reaction-plane resolution is defined as $\langle \cos n(\psi_n^{\text{meas}} - \psi_n^{\text{real}})\rangle$ [19]. The value of v_n^{meas} is obtained by fitting the azimuthal distribution (relative to the reaction plane) with

$$\frac{dN}{d\phi} = N_0\left[1 + 2v_n^{\text{meas}}\cos(n\phi)\right], \tag{4}$$

where N_0 and v_n^{meas} are fitting parameters. We can also calculate v_n^{meas} directly by

$$v_n^{\text{meas}} = \langle \cos(n\phi)\rangle. \tag{5}$$

In this analysis the v_2 is estimated by using the reaction plane found from the second harmonic ($n = 2$), since better accuracy of v_n is obtained by using the same harmonic's reaction plane [19]. The reaction planes are determined by using both BBCs. In the PHENIX experiment the reaction plane is also determined by using the central arm detectors. One of the key issues of the reaction-plane determination involves nonflow effects such as jets, resonance decays, and Hanbury-Brown and Twiss (HBT). Since each BBC is roughly three units of pseudorapidity away from the central arms, it is expected that the nonflow effects are smaller there than in the central arm detectors [2].

Using the BBC information the reaction plane is measured by

$$\psi = \left[\tan^{-1}\frac{\sum_{i=1}^{64} q_i \sin(2\phi_i)}{\sum_{i=1}^{64} q_i \cos(2\phi_i)}\right] \Big/ 2, \tag{6}$$

where ϕ_i is the azimuthal angle of each PMT and q_i is the charge information of each PMT. Owing to the random distribution of the impact-parameter direction in collisions, the reaction plane should have an isotropic azimuthal distribution. Because of the possible azimuthal asymmetries in the BBC response, however, the measured reaction-plane distribution is anisotropic. In this paper, we use the following two-step method to correct the reaction plane. First, the distribution of $\sum_{i=1}^{64} q_i \sin(2\phi_i)$ and $\sum_{i=1}^{64} q_i \cos(2\phi_i)$ are recentered by subtracting $\langle\sum_{i=1}^{64} q_i \sin(2\phi_i)\rangle$ and $\langle\sum_{i=1}^{64} q_i \cos(2\phi_i)\rangle$ over all events [19]:

$$\psi = \left[\tan^{-1}\frac{\sum_{i=1}^{64} q_i \sin(2\phi_i) - \left\langle\sum_{i=1}^{64} q_i \sin(2\phi_i)\right\rangle}{\sum_{i=1}^{64} q_i \cos(2\phi_i) - \left\langle\sum_{i=1}^{64} q_i \cos(2\phi_i)\right\rangle}\right] \Big/ 2. \tag{7}$$

This method does not remove higher harmonic components of the determined reaction plane, so we apply an additional correction method [20]. In this method flattening the reaction plane is accomplished by using a shift

$$n\psi^{\text{flat}} = n\psi_{\text{obs}} + \Delta\psi, \tag{8}$$

where $\Delta\psi$ is the correction factor for the reaction plane. $\Delta\psi$ is determined by

$$\Delta\psi = \sum_n A_n \cos(2n\psi_{\text{obs}}) + B_n \sin(2n\psi_{\text{obs}}), \tag{9}$$

where A_n and B_n are defined by requiring the nth Fourier moment of the new reaction plane (ψ^{flat}) to vanish. Hence

$$A_n = -\frac{2}{n}\langle \sin(2n\psi_{\text{obs}})\rangle, \tag{10}$$

$$B_n = \frac{2}{n}\langle \cos(2n\psi_{\text{obs}})\rangle. \tag{11}$$

Since the reaction plane depends on collision centrality and the z vertex, the reaction planes are divided into 40 samples (20 centrality bins and 2 vertex bins), and these corrections are determined independently for each sample. To measure the v_2 in this analysis, use is made of a combined reaction-plane, which is defined by weighted averaging of the

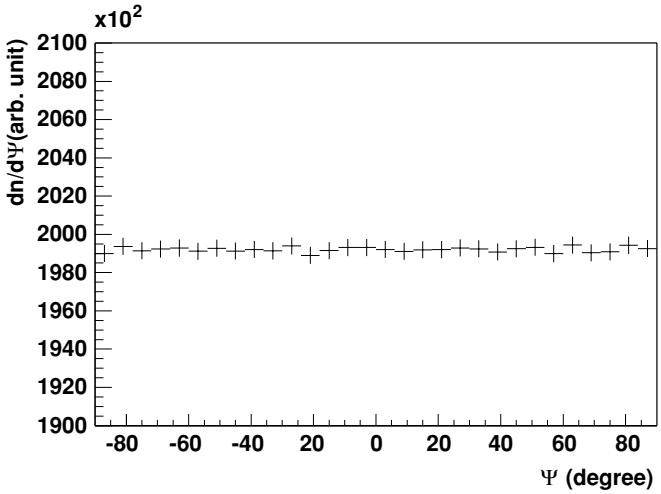

FIG. 3. The azimuthal angle distribution of the combined reaction plane after applying the flattening corrections. (Note that the vertical scale is zero suppressed.) After applying the corrections, the reaction plane has an isotropic azimuthal distribution.

reaction-plane angles obtained by the south-side BBC and the north-side BBC. Figure 3 shows the azimuthal angle distribution of the combined reaction plane after applying the flattening corrections. After applying the corrections, the reaction plane has an isotropic azimuthal distribution. The resolution of the combined reaction plane is estimated by using Eq. 11 in [19]. Figure 4 shows the centrality dependence of the resolution (σ_{v_2}).

III. RESULTS AND DISCUSSION

In this section we present a method to calculate the single-electron v_2 from inclusive electrons and show its transverse momentum dependence.

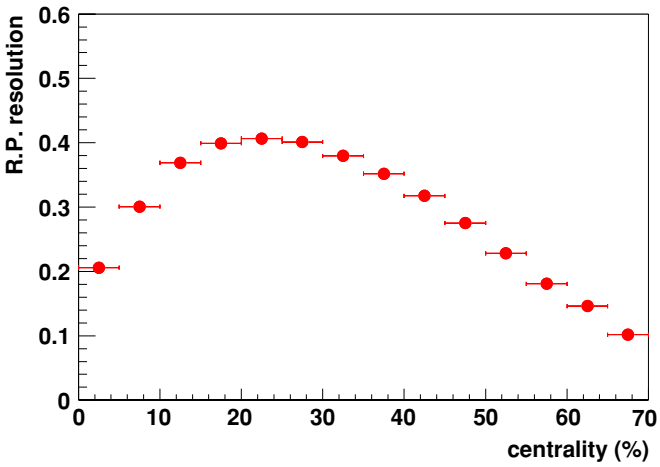

FIG. 4. (Color online) Centrality dependence of the combined reaction plane (R.P.) resolution determined by the BBC. The resolution is estimated by using Eq. 11 in [19].

A. Inclusive electron v_2

The azimuthal distributions of electrons relative to the reaction plane are shown in the middle panel of Fig. 5. The distributions are overlaid by shifting them on the vertical axis such that the spacing between each is equal. Each symbol represents the measured p_T region indicated in the left panel, which shows the raw yields of each distribution with large symbols. As described in Sec. II C, less than 10% background remains from accidental RICH associations. The azimuthal distributions of the background are shown in the right panel, and the yields are shown as small symbols in the left panel. The electron v_2 are measured after subtraction of this background ($dN^{e_{\rm back}}/d\phi$) from electrons that are identified by the RICH ($dN^{e_{\rm cand}}/d\phi$):

$$\frac{dN^e}{d\phi} = \frac{dN^{e_{\rm cand}}}{d\phi} - \frac{dN^{e_{\rm back}}}{d\phi}. \tag{12}$$

The transverse momentum dependence of the electron v_2 for minimum-bias events (centrality 0–92%) after subtracting background is shown in Fig. 6. The statistical errors are shown as vertical lines in the figure. The 1σ systematic uncertainties are shown as vertical bands. The systematic uncertainties include the systematic uncertainty of the reaction-plane determination and electron identification. The systematic uncertainty of the reaction-plane determination is about 5%. The uncertainty was estimated by measuring v_2 with a reaction plane determined by the north-side BBC, the south-side BBC, and a combination of the north and south sides. The systematic uncertainty from electron identification was estimated by measuring electron v_2 with several different sets of electron identification cuts. A comparison with v_2 for a charged pion [2] is also shown in Fig. 6. At low p_T ($p_T < 1.0$ GeV/c), the electron v_2 is larger than the v_2 of the pion. In this region electrons come mainly from π^0 decays, directly from the Dalitz decays, or indirectly from photon conversions. Because the decay angle of the π^0 decay is small, the electron has about the same azimuthal angle as the parent π^0, wheres the electron p_T is smaller than the π^0 p_T. Therefore the electron v_2 at a given p_T corresponds to the larger v_2 of the π^0 at higher p_T. The v_2 of charged pions is consistent with that of neutral pions [12]; therefore the inclusive electron v_2 is higher than the pion v_2. The v_2 at high p_T is thought to reflect parton energy loss in the initial stage of the collisions [21]. As described in Sec. III B, the primary source of electrons at high p_T is semileptonic decays of mesons containing heavy quarks. If these heavy quarks experience energy loss, the trend of the electron v_2 at high p_T might be the same as for pions. However, the electron v_2 at high p_T might be smaller than the pion v_2 if the heavy quarks do not lose energy. Owing to the large systematic and statistical uncertainty of the current measurement, the electron v_2 is consistent with the pion v_2.

B. Heavy-flavor electron v_2

The inclusive electron sample has two components: (1) a nonphotonic component, consisting of primarily semi-leptonic decays of mesons containing heavy (charm and bottom) quarks, and (2) a photonic component, consisting of Dalitz

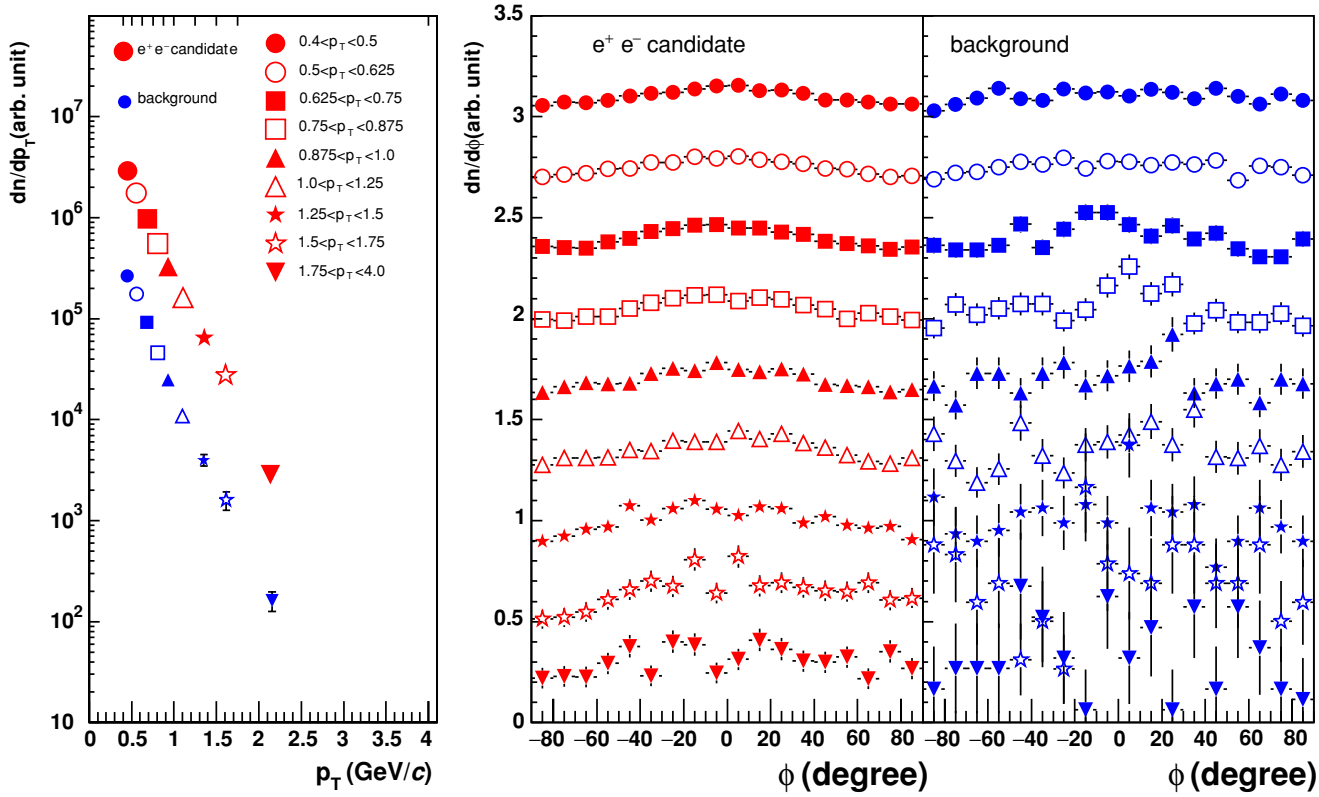

FIG. 5. (Color online) Azimuthal distributions relative to the reaction plane of electrons (middle panel) and the background (right panel) in each momentum bin. The distributions are overlaid by shifting them on the vertical axis such that the spacing between each is equal. The raw yields of each distribution are shown in the left panel.

decays of light neutral mesons (π_0, η, η', ω, and ϕ) and photon conversions in the detector material [9]. The azimuthal distribution of electrons ($dN^e/d\phi$) is the sum of the azimuthal distributions of photonic electrons ($dN^\gamma/d\phi$) and nonphotonic electrons ($dN^{\text{non}-\gamma}/d\phi$):

$$\frac{dN_e}{d\phi} = \frac{dN_e^\gamma}{d\phi} + \frac{dN_e^{\text{non}-\gamma}}{d\phi}. \tag{13}$$

The second harmonic of the Fourier expansion of each azimuthal distribution is defined according to

$$\begin{aligned} &N_e\left[1 + 2v_{2_e}\cos(2\phi)\right] \\ &= N_e^\gamma\left[1 + 2v_{2_e}^\gamma\cos(2\phi)\right] + N_e^{\text{non}-\gamma}\left[1 + 2v_{2_e}^{\text{non}-\gamma}\cos(2\phi)\right] \\ &= \left(N_e^\gamma + N_e^{\text{non}-\gamma}\right)\left[1 + 2\frac{N_e^\gamma v_{2_e}^\gamma + N_e^{\text{non}-\gamma}v_{2_e}^{\text{non}-\gamma}}{N_e^\gamma + N_e^{\text{non}-\gamma}}\cos(2\phi)\right], \end{aligned} \tag{14}$$

where v_{2_e} is the v_2 of inclusive electron, $v_{2_e}^\gamma$ is the v_2 of the photonic electrons, and $v_{2_e}^{\text{non}-\gamma}$ is the v_2 of the nonphotonic electrons. From Eq. (14), the inclusive electron v_2 is given by

$$\begin{aligned} v_{2_e} &= \frac{N_e^\gamma v_{2_e}^\gamma + N_e^{\text{non}-\gamma}v_{2_e}^{\text{non}-\gamma}}{N_e^\gamma + N_e^{\text{non}-\gamma}} \\ &= \frac{N_e^\gamma v_{2_e}^\gamma + \left(N_e - N_e^\gamma\right)v_{2_e}^{\text{non}-\gamma}}{N_e} \\ &= r v_{2_e}^\gamma + (1-r)v_{2_e}^{\text{non}-\gamma}, \end{aligned} \tag{15}$$

where r is defined as $r = 1/(1 + R_{\text{NP}})$, and R_{NP} is the ratio of the number of nonphotonic electrons to photonic electrons

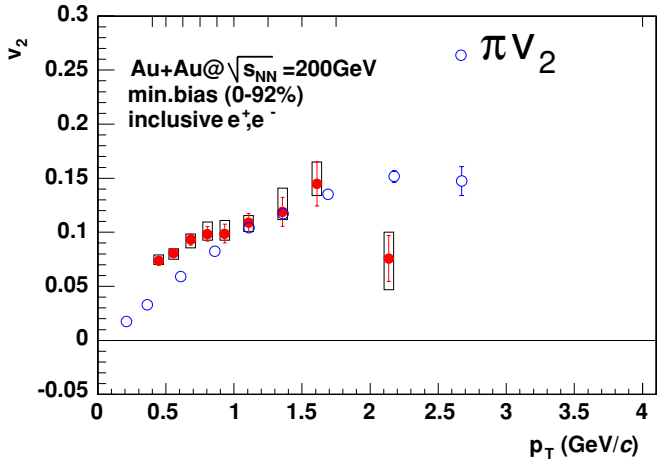

FIG. 6. (Color online) Transverse momentum dependence of the electron v_2 for minimum-bias events (centrality 0–92%). The data points for the electrons represent the inclusive single electrons (e^+ and e^-). The upper horizontal scale shows the bin size in p_T. The statistical errors are shown as vertical lines in the figure. The systematic uncertainty from the determination of the reaction plane and electron identification are shown as boxes. A comparison with the pionπ v_2 is also shown.

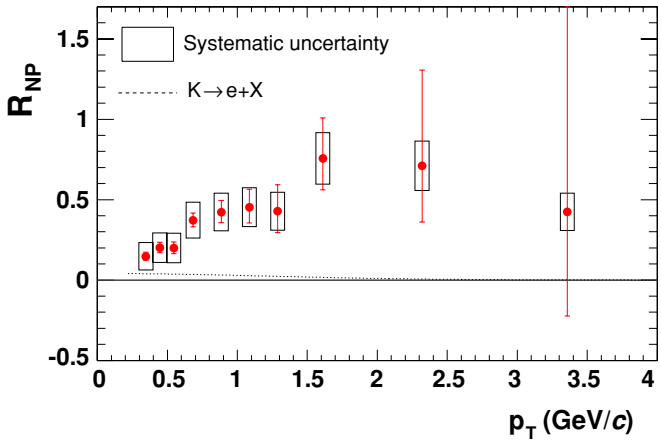

FIG. 7. (Color online) Ratio of nonphotonic to photonic $e^{\pm}$ yields ($R_{\rm NP}$, points) and contribution from kaon decays (dashed line) [9].

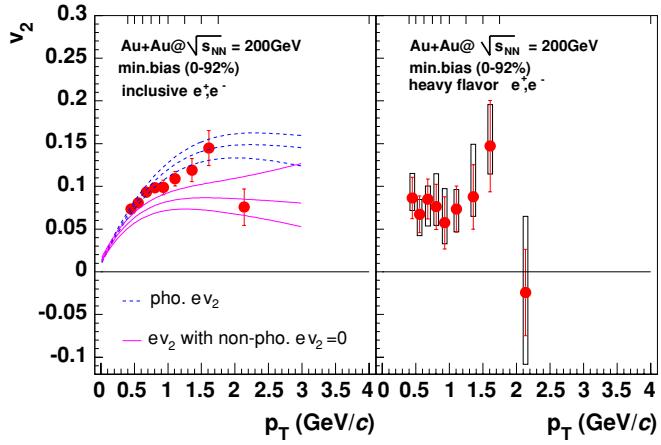

FIG. 8. (Color online) (Left) A comparison of the inclusive electron v_2 with the photonic electron v_2 (dashed line). The solid line is $r v_{2_e^\gamma}$, the photonic electron v_2 scaled by the ratio of the number of inclusive to photonic electrons. The electron v_2 is the same as $r v_{2_e^\gamma}$ if the nonphotonic electron v_2 is zero; that is, the v_2 of the parent particle, such as a D meson, is zero. (Right) Transverse momentum dependence of the heavy quark electron v_2 for minimum-bias events. The vertical line is the statistical error, which is propagated from the statistical errors of the electron v_2 for minimum-bias events. The systematic uncertainty from the electron v_2, the photonic electron v_2, and the ratio $R_{\rm NP}$ is shown as a band.

($N_e^{\rm non-\gamma}/N_e^{\gamma}$). We experimentally determined the ratio from analysis of special runs in which an additional an photon converter was installed. The details of the method are described in [9], and the measured ratio is shown in Fig. 7. The increase in the number of nonphotonic electrons is consistent with that expected from semileptonic charm decays [9]. From Eq. (15) $v_{2_e}^{\rm non-\gamma}$ can be expressed as

$$v_{2_e}^{\rm non-\gamma} = \frac{v_{2_e} - r v_{2_e}^{\gamma}}{1 - r}. \tag{16}$$

The dominant sources of photonic electrons are photon conversions and Dalitz decays from π^0 [8]. In addition, we also took into account electrons from η decays when calculating photonic electron v_2. We assumed that the contributions from η decays is 17% by taking into account $\eta/\pi_0 = 0.45$ [9]. The other sources are ignored when calculating the photonic electron v_2 because of their small contribution. The decay electron v_2 from decay electrons of π^0 and η were calculated by Monte Carlo simulation. The transverse momentum dependence of the $\pi^0 v_2$ was obtained from the measured $\pi^0 v_2$ [12] ($p_T > 1.0$ GeV/c) and the measured charged pion v_2 ($p_T < 1.0$ GeV/c). Both measurements were used since the $\pi^0 v_2$ has been measured only above 1.0 GeV/c, and both v_2 measurements are consistent at intermediate p_T ($1.0 < p_T < 3.0$). The measured π^0 spectra [22] were used to give the input transverse momentum spectrum. We assumed that the transverse momentum dependence of the η v_2 is the same as for the kaon v_2 because their mass difference is small. The transverse momentum spectrum of η was approximated by assuming m_T scaling of π^0 spectra. The photonic electron v_2 calculated from the results is shown as the dashed line in the left panel of Fig. 8. The middle dashed line is the mean value of the photonic electron v_2 and the upper and lower dashed lines show the 1σ systematic uncertainty. The systematic uncertainty of the photonic electron v_2 was estimated from the statistical error and the systematic error of the measured parent v_2. If the nonphotonic electron v_2 is zero, that means the v_2 of the parent particle, such as a D meson, is zero. Additionally, the inclusive electron v_2 is the same as that of the scaled photonic electron ($r v_{2_e^\gamma}$) from Eq. (15). The scaled photonic electron v_2 is shown as the solid line in the left panel in Fig. 8. At intermediate p_T ($1.0 < p_T < 1.5$) the electron v_2 is higher than $r v_{2_e^\gamma}$. This might suggest that the nonphotonic electron has nonzero v_2 at intermediate p_T. The details of this discussion are presented in the next section.

Background from kaon decays ($K \to \pi\ e\ \nu$) remains in the nonphotonic yield. The contribution of kaon decays to the nonphotonic yield, shown in Fig. 7 as a dashed line, is 18% at $p_T = 0.4$ GeV/c and decreases rapidly to less than 6% for $p_T = 1$ GeV/c [9]. The transverse momentum dependence of the kaon v_2 has been measured up to 3.0 GeV/c and that of the K_S^0 v_2 has been measured up to 6.0 GeV/c [5]. The kaon and K_S^0 v_2 are consistent up to 3.0 GeV/c, and the quark coalescence model predicts that these two meson v_2 values are the same. Therefore, kaon and K_S^0 v_2 were combined as input for the kaon v_2. The transverse momentum spectrum of kaons was obtained from measured kaon spectra up to 2.0 GeV/c. In the high-p_T region we used scaled π^0 spectra and assumed that the shapes of the kaon spectra were the same as for the π^0 spectra, which are matched with measured kaon spectra around 2.0 GeV/c.

The nonphotonic electrons mainly come from semileptonic decays of heavy flavor (charm and beauty). Therefore the non-photonic electron v_2 that was obtained by subtracting photonic electron and kaon decays from inclusive electrons should be heavy-flavor electron [9] v_2, which reflects the azimuthal anisotropy of heavy quarks. The result of the heavy-flavor electron v_2 for minimum-bias events is shown in the right panel of Fig. 8. The vertical lines are the statistical errors that are propagated from the statistical errors of the inclusive

TABLE I. The relative systematic uncertainty of heavy-quark electron v_2.

p_T Range	Systematic Error Bound	Inclusive ev_2 (%)	Photonic ev_2 (%)	R_{NP} (%)	R.P. (%)	Total (%)
$0.4 < p_T < 1.0$	lower	<32	<26	<21	4.5	<42
	upper	<63	<21	<21	4.5	<70
$1.0 < p_T < 1.75$	lower	<25	<21	<14	4.5	<36
	upper	<67	<17	<15	4.5	<70
$1.75 < p_T < 4.0$	lower	280	78	190	4.5	340
	upper	220	64	280	4.5	360
Type		A	A	A	B	

electron v_2 shown in Fig. 6. The 1σ systematic uncertainties of heavy-flavor electron v_2 are shown as bands. The systematic uncertainty includes the systematic uncertainty of the reaction plane, the measured inclusive electron v_2 (without the reaction plane), the photonic electron v_2 (without the reaction plane), and R_{NP}. The systematic uncertainty of R_{NP} is the quadratic sum of the statistical and systematic errors because R_{NP} is measured with a different data set. There are two categories of uncertainty: Type A is a point-to-point error uncorrected between p_T bins, and type B is a common displacement of all points by the same factor independent of p_T. The total systematic uncertainty is calculated by propagating the errors on the individual quantities that enter into Eq. (16). Table I shows the relative systematic uncertainty of heavy-quark electron v_2.

From the result we calculated the confidence level for a nonzero v_2. We assumed that the data of measured heavy-flavor electron v_2 follow a Gaussian distribution; the σ was obtained by calculating the quadratic sum of the statistical and systematic errors of the heavy-flavor electron v_2 assuming these errors to be independent. In the intermediate-p_T region ($1.0\ \text{GeV}/c < p_T < 1.75\ \text{GeV}/c$), the confidence level for a nonzero value for the measured heavy-flavor electron v_2 is 90%.

There are various scenarios to consider that lead to different elliptic flow values for D mesons [14]. One is that the charm quarks do not interact at all in the medium after being produced and eventually fragment in vacuum into D mesons. This scenario leads to zero elliptic flow ($v_2 = 0$). It is also possible that charm quarks do not flow with the medium but do suffer energy loss in the medium and then eventually fragment in vacuum into D mesons. This scenario may yield a nonzero v_2. Alternatively, the charm quarks may flow in the medium and then hadronize via coalescence or recombination with other partons from the medium, which could produce significant nonzero values for v_2. Finally, even if the charm quarks do not flow with the medium, but do hadronize via recombination, they may pick up some v_2 from the light quarks in the medium.

By assuming the quark coalescence model, the decay electron v_2 from D mesons has been predicted [10]. In the model D mesons are formed from charm quark coalescence with thermal light quarks at hadronization. For charm quark momentum spectra, two extreme scenarios are considered. The first scenario assumes no reinteractions after the production of charm-anticharm quark pairs in initial-state hard processes (calculated from PYTHIA). The second scenario assumes complete thermalization with the transverse flow of the bulk matter. Figure 9 shows a comparison of the heavy-flavor electron v_2 with decay electrons from D mesons in the "no reinteraction" scenario as a solid line; the dashed line reflects the "thermalization" scenario. Because of large systematic and statistical uncertainty of the current measurement, neither scenario is excluded by this single-electron v_2 measurement.

IV. SUMMARY

In summary, we have measured the elliptic flow, v_2, of single electrons from heavy-flavor decay. This single-electron v_2 is produced by subtracting the v_2 of electron sources such as photon conversion from the v_2 of inclusive electrons measured with the PHENIX detector in Au+Au collisions at $\sqrt{s_{NN}} = 200$ GeV with respect to the reaction plane defined at high rapidities ($|\eta| = 3$–4). The measured heavy-flavor electron v_2 is nonzero with a 90% confidence level. Two model calculations from [10] assume extremely different scenarios: either no reinteraction of the initially produced charm quarks or complete thermalization with the bulk matter. Both of these calculations are consistent within errors with the measured heavy-flavor electron v_2.

High-luminosity Au+Au collisions at $\sqrt{s_{NN}} = 200$ GeV have been recorded by the PHENIX experiment during Run4

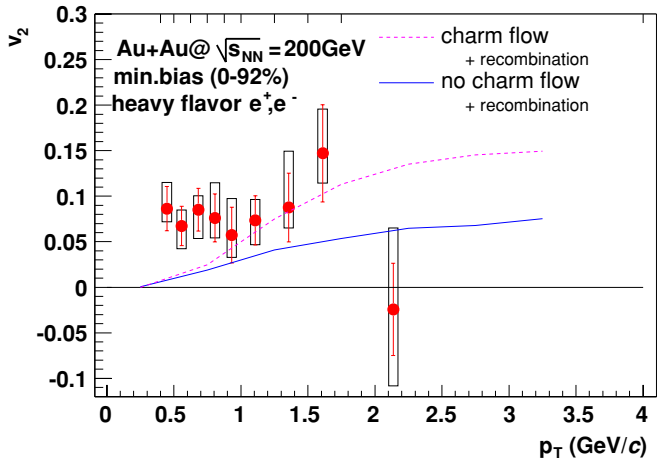

FIG. 9. (Color online) Comparison of the heavy-flavor electron v_2 with two different charm flow scenarios from [10]. The solid line corresponds to no rescattering of the initially produced charm quarks (without flow); the dashed line reflects the effect of complete thermalization (with flow).

(2003–2004). The much higher statistical precision of these data should allow an unambiguous result on the important issue of charm flow.

ACKNOWLEDGMENTS

We thank the staff of the Collider-Accelerator and Physics Departments at Brookhaven National Laboratory and the staff of the other PHENIX participating institutions for their vital contributions. We acknowledge support from the Department of Energy, Office of Science, Nuclear Physics Division, the National Science Foundation, Abilene Christian University Research Council, Research Foundation of SUNY, and Dean of the College of Arts and Sciences, Vanderbilt University (USA); Ministry of Education, Culture, Sports, Science, and Technology and the Japan Society for the Promotion of Science (Japan); Conselho Nacional de Desenvolvimento Científico e Tecnológico and Fundac oa de Amparo à Pesquisa do Estado de São Paulo (Brazil); Natural Science Foundation of China (People's Republic of China); Centre National de la Recherche Scientifique, Commissariat à l'Éenergie Atomique, Institut National de Physique Nucléaire et de Physique des Particules, and Institut National de Physique Nucléaire et de Physique des Particules (France); Bundesministerium für Bildung und Forschung, Deutscher Akademischer Austausch Dienst, and Alexander von Humboldt Stiftung (Germany); Hungarian National Science Fund, OTKA (Hungary); Department of Atomic Energy and Department of Science and Technology (India); Israel Science Foundation (Israel); Korea Research Foundation and Center for High Energy Physics (Korea), Russian Ministry of Industry, Science and Tekhnologies, Russian Academy of Science, and Russian Ministry of Atomic Energy (Russia), Vetenskapsrådet/Swedish Research Council (VR) and the Wallenberg Foundation (Sweden), the U.S. Civilian Research and Development Foundation for the Independent States of the Former Soviet Union; the US-Hungarian NSF-OTKA-MTA; the US-Israel Binational Science Foundation; and the 5th European Union TMR Marie-Curie Programme.

[1] H. Sorge, Phys. Rev. Lett. **82**, 2048 (1999).
[2] S. S. Adler *et al*. (PHENIX Collaboration), Phys. Rev. Lett. **91**, 182301 (2003).
[3] J. Adams *et al*. (STAR Collaboration), Phys. Rev. Lett. **87**, 182301 (2001).
[4] J. Adams *et al*. (STAR Collaboration), Phys. Rev. Lett. **89**, 132301 (2002).
[5] J. Adams *et al*. (STAR Collaboration), Phys. Rev. Lett. **92**, 052302 (2004).
[6] P. Houvinen, P. E. Kolb, U. W. Heinz, P. V. Ruuskanen, and S. A. Voloshin, Phys. Lett. **B503**, 58 (2001).
[7] D. Molnar and S. A. Voloshin, Phys. Rev. Lett. **91**, 092301 (2003).
[8] K. Adcox *et al*., Phys. Rev. Lett. **88**, 192303 (2002).
[9] S. S. Adler *et al*. (PHENIX Collaboration), Phys. Rev. Lett. **94**, 082301 (2005).
[10] V. Greco, C. M. Ko, and R. Rapp, Phys. Lett. **B595**, 202 (2004).
[11] X. Dong, S. Esumi, P. Sorensen, N. Xu, and Z. Xu, Phys. Lett. **B597**, 328 (2004).
[12] M. Kaneta *et al*., *Proceedings of the 17th International Conference Ultra Relativistic Nucleus-Nucleus Collisions (Quark Matter 2004)*; J. Phys. G **30**, S1217 (2004); nucl-ex/0404014.
[13] F. Laue, Proceedings of Hot Quarks 2004: Workshop for Young Scientists on the Physics of Ultrarelativistic Nucleus-Nucleus Collisions (HQ'04); J. Phys. G **31**, S27 (2005); nucl-ex/0411007.
[14] S. Batsouli *et al*., Phys. Lett. **B577**, 26 (2003).
[15] K. Adcox *et al*., Nucl. Instrum. Methods Phys. Res. A **499**, 469 (2003).
[16] S. H. Aronson *et al*. (PHENIX Collaboration), Nucl. Instrum. Methods Phys. Res. A **499**, 480 (2003).
[17] S. S Adler *et al*. (PHENIX Collaboration), Phys. Rev. Lett. **91**, 072301 (2003).
[18] J. T. Mitchell *et al*. (PHENIX Collaboration), Nucl. Instrum. Methods Phys. Res. A **482**, 491 (2002).
[19] A. M. Poskanzer and S. A. Voloshin, Phys. Rev. C **58**, 1671 (1998).
[20] J. Barrette *et al*. (E877 Collaboration), Phys. Rev. C **56**, 3254 (1998).
[21] M. Gyulassy, I. Vitev, and X.-N. Wang, Phys. Rev. Lett. **86**, 2537 (2001).
[22] S. S. Adler *et al*., Phys. Rev. Lett. **89**, 202301 (2002).